

## **Supporting Information file**

### **Influence of Keto-Enol Tautomerism in Regulating CO<sub>2</sub> Photoreduction Activity in Porous Organic Porphyrinic Photopolymer**

Ankita Boruah,<sup>†,‡</sup> Bishal Boro,<sup>†,‡</sup> Jiarui Wang,<sup>§</sup> Ratul Paul,<sup>†</sup> Rajib Ghosh,<sup>€</sup> Debansh Mohapatra,<sup>‡</sup> Pei-Zhou Li,<sup>§\*</sup> Xinglong Zhang,<sup>‡, Δ\*</sup> and John Mondal<sup>†,‡\*</sup>

<sup>†</sup>Department of Catalysis & Fine Chemicals, CSIR- Indian Institute of Chemical Technology, Uppal Road, Telangana State, Hyderabad-500007, India. Email: [johncuchem@gmail.com](mailto:johncuchem@gmail.com);

[johnmondal@iict.res.in](mailto:johnmondal@iict.res.in)

<sup>‡</sup>Academy of Scientific and Innovative Research (AcSIR), Ghaziabad-201001, India.

<sup>§</sup>School of Chemistry and Chemical Engineering, Shandong University, Jinan 250100, Shandong Province, People's Republic of China. E-mail: [pzli@sdu.edu.cn](mailto:pzli@sdu.edu.cn)

<sup>€</sup>Radiation and Photochemistry Division, Bhabha Atomic Research Centre, Mod. Lab, Trombay, Mumbai-400085, India.

<sup>‡</sup>Department of Chemical Sciences, Indian Institute of Science Education and Research Berhampur Transit Campus (Govt. ITI Building), Engineering School Road, Berhampur 760010, Odisha, India

<sup>‡</sup>Department of Chemistry, The Chinese University of Hong Kong, Shatin, New Territories, 999077 Hong Kong, Special Administration Region of the People's Republic of China.

E-mail: [xinglong.zhang@cuhk.edu.hk](mailto:xinglong.zhang@cuhk.edu.hk)

<sup>Δ</sup>Institute of High-Performance Computing, Agency for Science, Technology and Research (A\*STAR), Singapore, 138632 Singapore.

\*Corresponding Author

## II. COMPUTATIONAL SECTION

### II.1 Computational Methods

Geometry optimizations were carried out using *Gaussian 16* rev. B.01 software,<sup>3</sup> in the gas phase using the global hybrid DFT functional M06-2X<sup>4</sup> and the def2-SVP<sup>5,6</sup> basis set for all atoms. Truhlar's M06-2X functional was chosen to study the present system, as this functional has been employed in the studies of a range of organic systems with good accuracy.<sup>7-15</sup> Minima and transition structures on the potential energy surface (PES) were confirmed as such by harmonic frequency analysis, showing respectively zero and one imaginary frequency.

To improve on the accuracy of the corrected Gibbs energy profile, single point (SP) calculations on the gas phase optimized geometries were performed at M06-2X with def2-TZVP<sup>5,6</sup> basis set for all atoms in the implicit C-PCM continuum solvation model<sup>16,17</sup> to model the effect of acetonitrile : water (4 : 1) mixed solvent that was used experimentally, on the potential energy surface. A linearly interpolated dielectric constant ( $\epsilon$ ) value of 44.22 for the solvent mixture was used ( $35.688 \times 0.8 + 78.3553 \times 0.2$ ). This value is close to the empirical dielectric constant of acetonitrile-water mixture ( $\epsilon = 43.1$  at 25 °C)<sup>18</sup> and we use simple linear interpolation for generality to other solvent mixtures for future work. Unless otherwise stated, the final corrected Gibbs energy C-PCM(acetonitrile-water)-M06-2X/def2-TZVP// M06-2X/def2-SVP is used for discussion throughout. All Gibbs energy values in the text and figures are quoted in eV.

Gibbs energies were evaluated at the reaction temperature of 25 °C, using Grimme's scheme of quasi-RRHO treatment of vibrational entropies<sup>19</sup>, using the GoodVibes code<sup>20</sup>. Vibrational entropies of frequencies below 100 cm<sup>-1</sup> were obtained according to a free rotor description, using a smooth damping function to interpolate between the two limiting descriptions.<sup>19</sup> The free energies reported in *Gaussian* from gas-phase optimization were further corrected using standard concentration of 1 mol/L,<sup>21</sup> which were used in solvation calculations, instead of the gas-phase 1atm used by default in the *Gaussian* program.

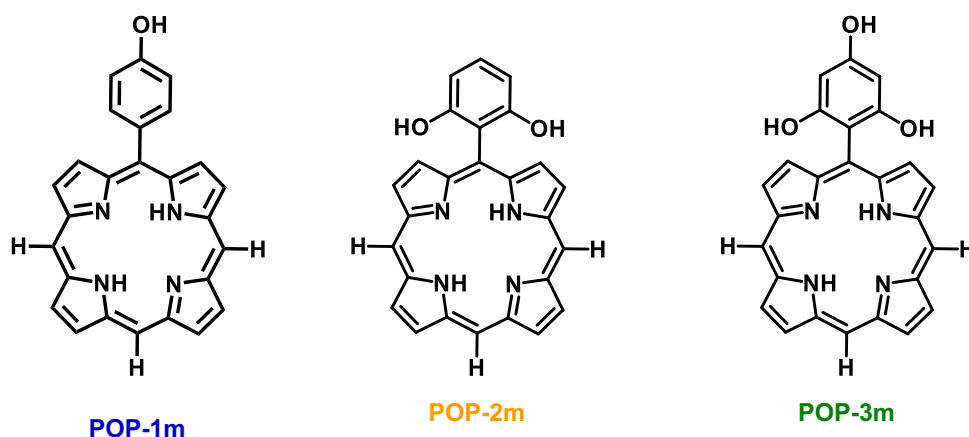
For time-dependent DFT (TD-DFT) calculations, CAM-B3LYP functional<sup>22</sup> was adopted due to its robust performance for the study of excited states.<sup>23-26</sup> We adopt def2-SVPD<sup>5,27</sup> basis set for all atoms for TD-DFT calculations. The "D" in def2-SVPD basis set denotes diffuse functions which are important for the correct description of anionic electron distributions and excited states.<sup>28-30</sup> For UV-vis spectra, a total of 50 excited states were included for calculations. The Gaussian function, with a standard deviation of wavenumber ( $\sigma$ ) of 0.4 eV, was used to broaden the peaks, as described on the *Gaussian 16* webpage.<sup>31</sup>

Molecular orbitals, spin density plots, electron density difference and electrostatic potential (ESP) maps are visualized using *PyMOL* software.<sup>32</sup>

### II.2 Model reaction

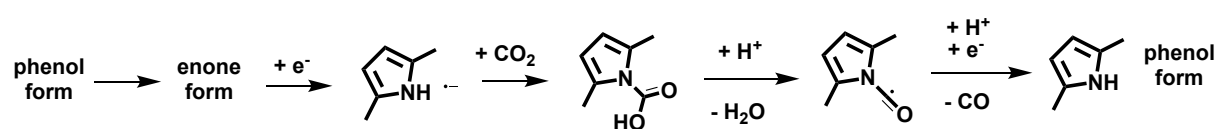
Scheme S4 shows the model reaction that we have used for the computational studies of reaction mechanism for POP-catalyzed CO<sub>2</sub> to CO conversion. **POP-1m** is the model system for **POP-1**,

**POP-2m** is the model system for **POP-2** and **POP-3m** is the model system for **POP-3**. The suffix “m” denotes model system.



**Scheme S4.** Model systems used in the computational modelling studies.

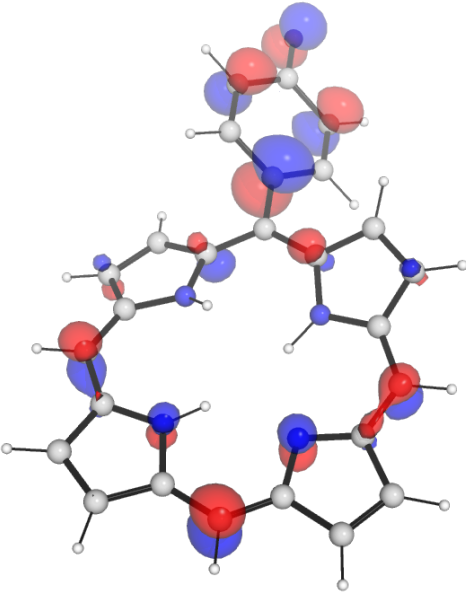
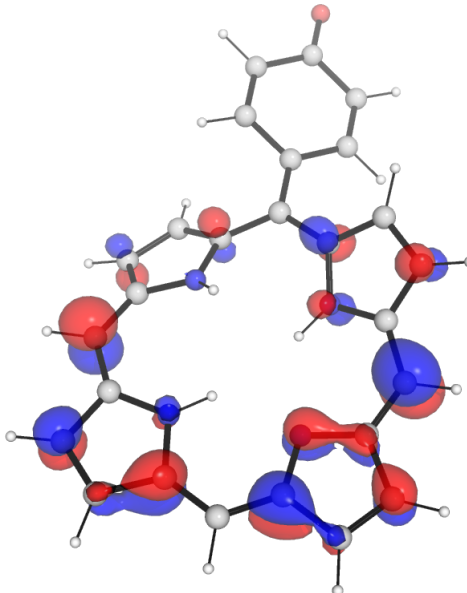
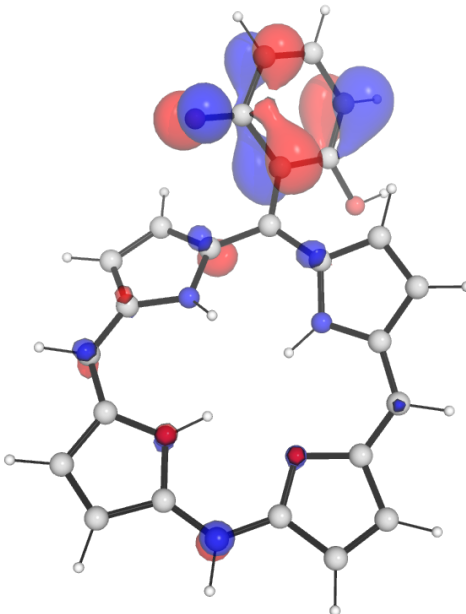
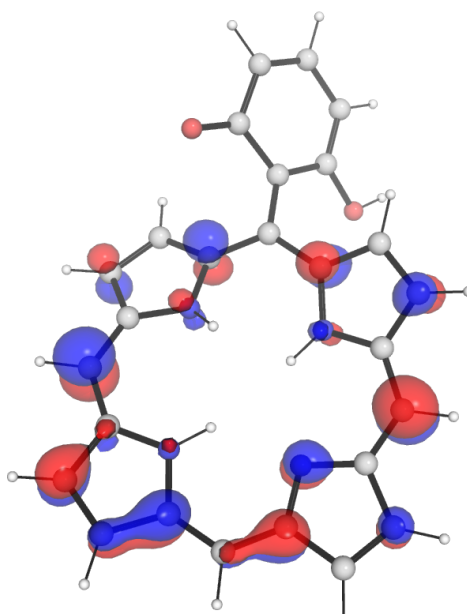
### II.3 Reaction mechanism

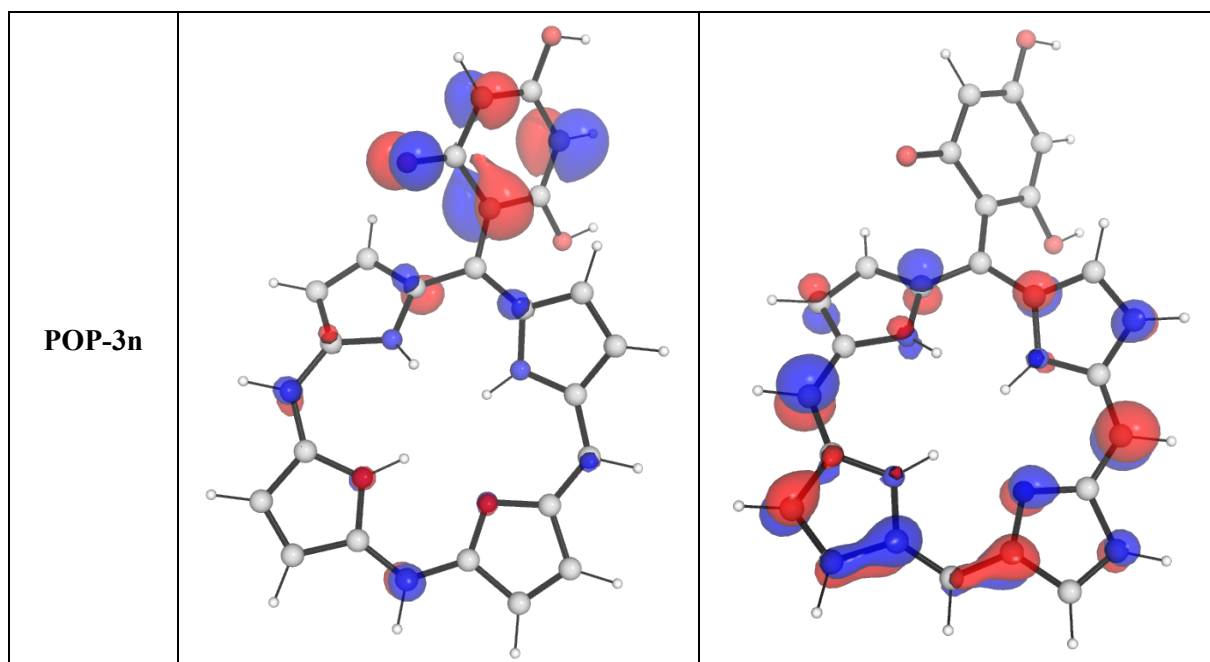


**Scheme S5.** Schematic representation of the catalytic cycle.

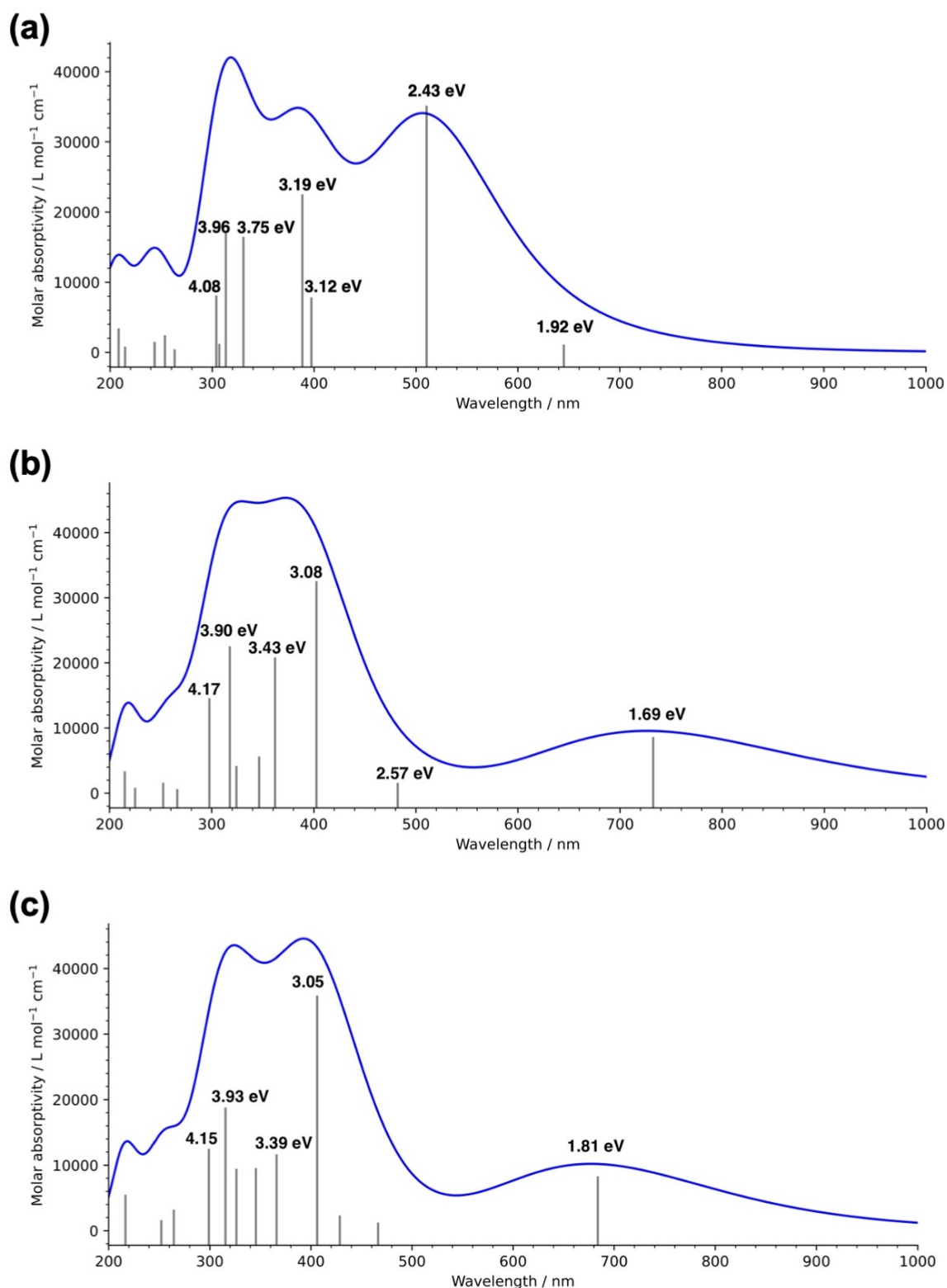
### II.4 DFT-optimized structures

Geometries of all optimized structures (in .xyz format with their associated energy in Hartrees) are included in a separate folder named *DFT\_optimized\_structures* with an associated readme.txt file. All these data have been deposited and uploaded to <https://zenodo.org/records/11408333> (DOI: 10.5281/zenodo.11408333).

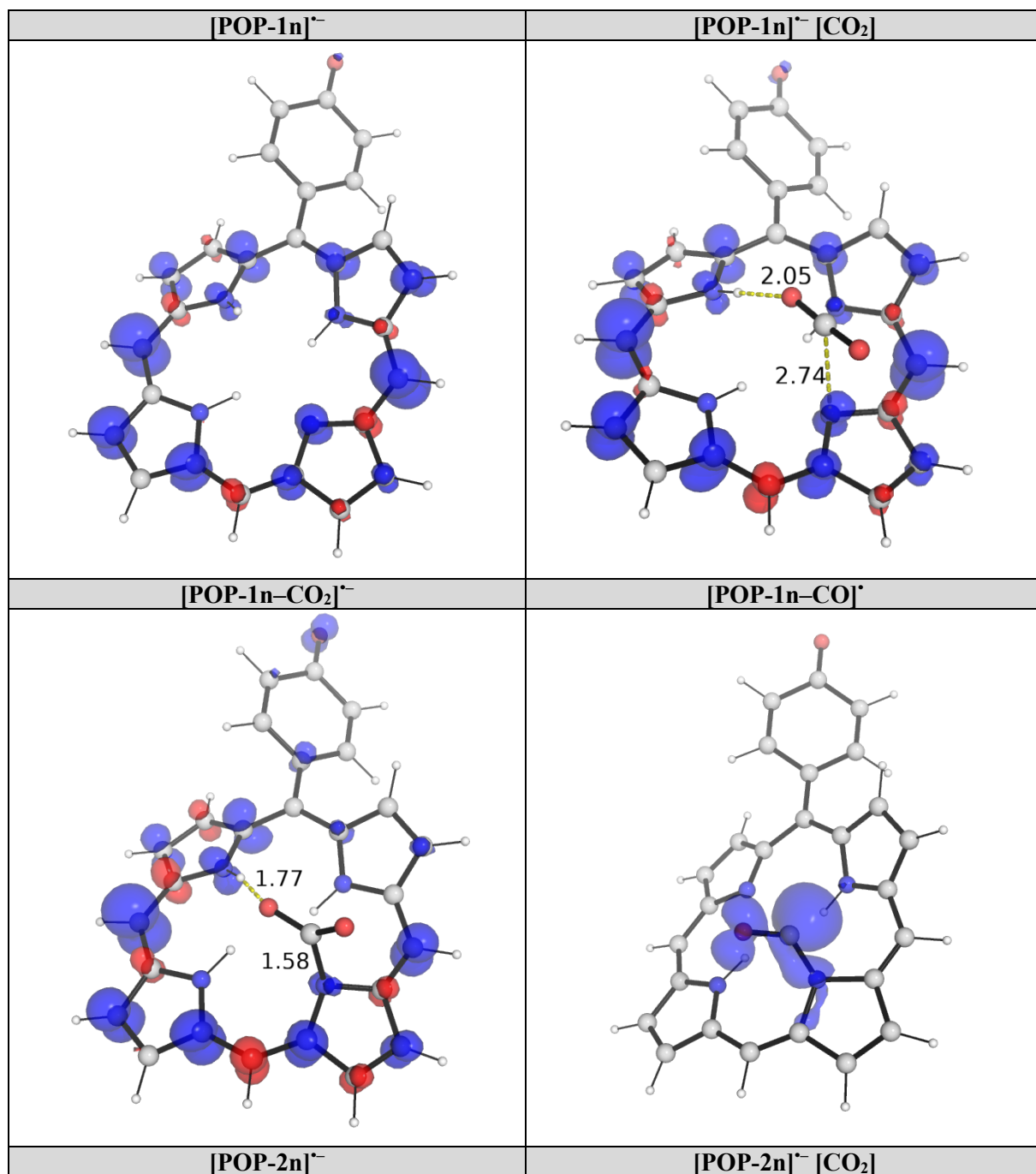
Structure	HOMO	LUMO
POP-1n	 <p>3D visualization of the Highest Occupied Molecular Orbital (HOMO) for POP-1n. The molecule is shown with red and blue isosurfaces representing the orbital lobes. The orbitals are primarily localized on the nitrogen-containing rings and the central carbon atom.</p>	 <p>3D visualization of the Lowest Unoccupied Molecular Orbital (LUMO) for POP-1n. The molecule is shown with red and blue isosurfaces. The orbitals are distributed across the entire structure, with significant lobes on the nitrogen-containing rings and the central carbon atom.</p>
POP-2n	 <p>3D visualization of the Highest Occupied Molecular Orbital (HOMO) for POP-2n. The molecule is shown with red and blue isosurfaces. The orbitals are primarily localized on the nitrogen-containing rings and the central carbon atom.</p>	 <p>3D visualization of the Lowest Unoccupied Molecular Orbital (LUMO) for POP-2n. The molecule is shown with red and blue isosurfaces. The orbitals are distributed across the entire structure, with significant lobes on the nitrogen-containing rings and the central carbon atom.</p>

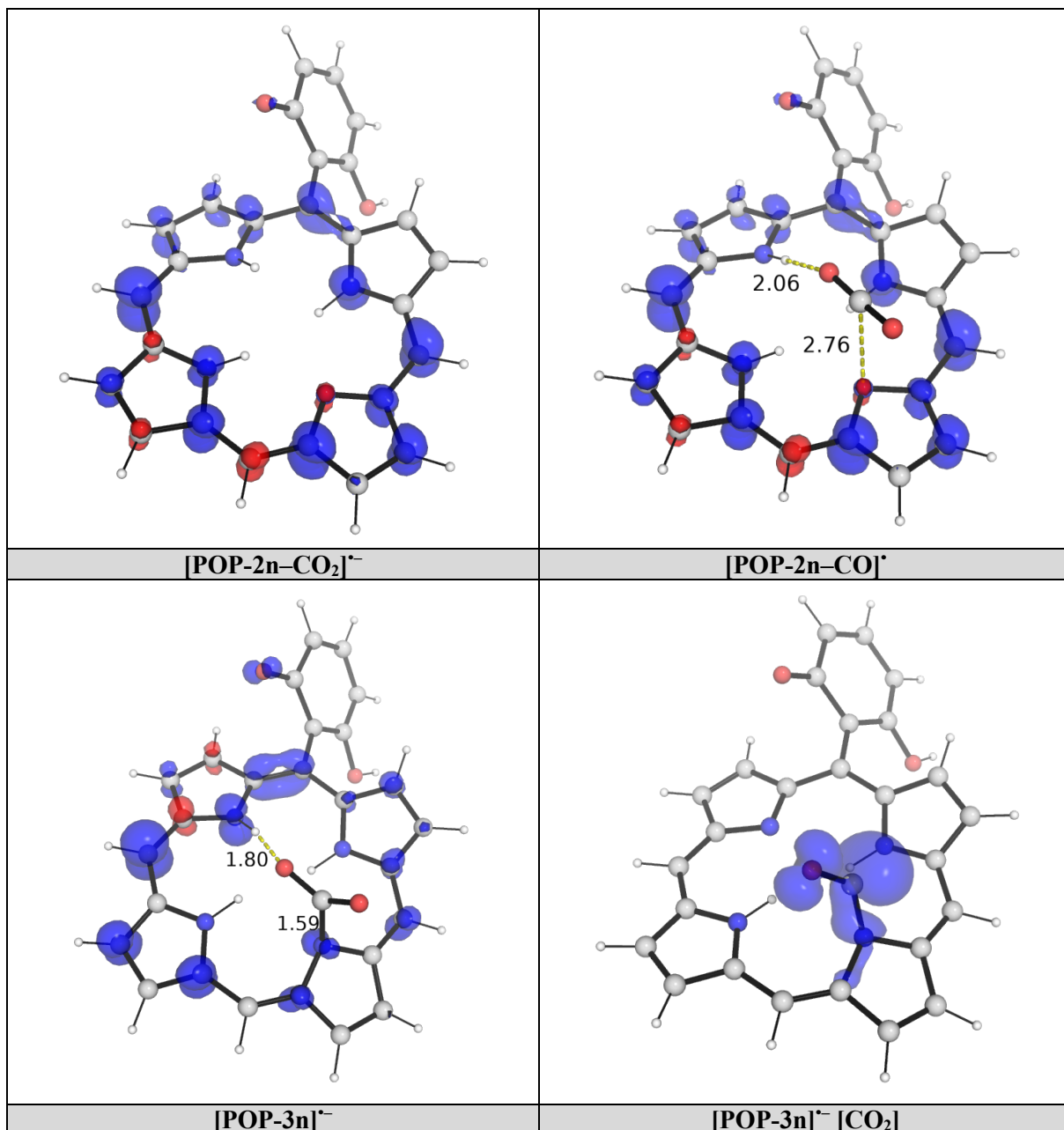


**Figure S19:** HOMO and LUMO structures for the enone forms of the POP model systems (“n” suffix denotes enone form). Molecular orbitals are shown at an isosurface value of 0.05 au.



**Figure S20:** Computed UV-Vis spectrum for model systems **POP-1n** (a), **POP-2n** (b) and **POP-3n** (c). Peaks were broadened by a wavenumber ( $\sigma$ ) of 0.4 eV. Only peaks with oscillatory strengths greater than or equal to 0.05 are shown.







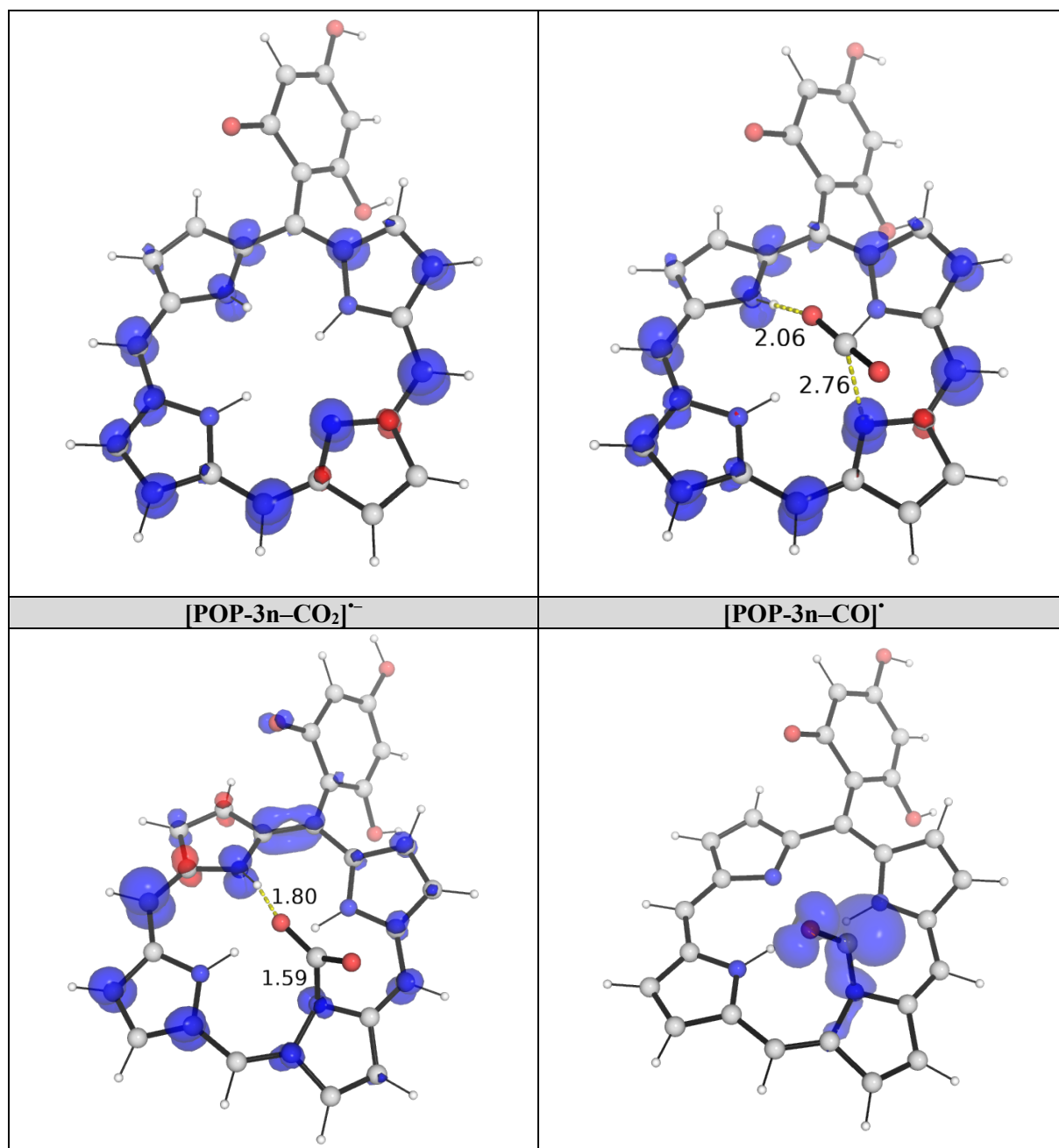


**Figure S21:** Spin density plots of the radical ionic species in the reaction. Spin densities are shown at an iso surface value of 0.005 au.

**Table S3:** Optimized structures and raw energy values. Absolute values (in Hartrees) for SCF energy, zero-point vibrational energy (ZPE), enthalpy and quasi-harmonic Gibbs free energy (at 25 °C/298.15 K) for optimized structures are given below. Single point corrections in SMD ethanol using M062X-def2-TZVP level of theory are also included. “rc” denotes radical cation and “ra” denotes radical anion.

Structure	E/au	ZPE/au	H/au	T.S/au	qh-G/au	SP M062X-def2-TZVP
TEOA	-517.42116	0.222877	-517.18467	0.050433	-517.233319	-518.04644
TEOA_rc	-517.14298	0.221347	-516.90758	0.052482	-516.957921	-517.83249
proton	0	0	0.00236	0.009341	-0.006981	-0.1629214
water	-76.323214	0.021589	-76.297846	0.019066	-76.316911	-76.433632
CO2	-188.37047	0.012131	-188.35478	0.021219	-188.376001	-188.59939
CO	-113.18564	0.00529	-113.17705	0.019401	-113.196447	-113.32287
POP-1m	-1294.3563	0.38496	-1293.9492	0.068703	-1294.014829	-1295.7888
POP-1n	-1294.4101	0.381797	-1294.0043	0.073593	-1294.074699	-1295.9058
POP-1n_ra	-1294.3975	0.381438	-1293.9922	0.073199	-1294.062365	-1295.888
POP-1n_ra-CO2	-1482.7861	0.394838	-1482.3634	0.083121	-1482.441741	-1484.4955
POP-1n-CO2_ra	-1482.7731	0.396805	-1482.35	0.078298	-1482.424764	-1484.4867
POP-1n-CO_radical	-1406.847	0.383126	-1406.4401	0.072481	-1406.509361	-1408.4172
POP-2m	-1369.5036	0.389754	-1369.089	0.074457	-1369.160199	-1371.026
POP-2n	-1369.4531	0.389434	-1369.0388	0.075032	-1369.110347	-1370.9866
POP-2n_ra	-1369.5304	0.386036	-1369.1191	0.07602	-1369.191815	-1371.1253
POP-2n_ra-CO2	-1557.9177	0.399478	-1557.489	0.086023	-1557.569947	-1559.7325
POP-2n-CO2_ra	-1557.9035	0.401064	-1557.4749	0.080985	-1557.55204	-1559.7182
POP-2n-CO_radical	-1481.9805	0.386637	-1481.5689	0.074924	-1481.640282	-1483.6444
POP-3m	-1444.6468	0.394216	-1444.2266	0.076953	-1444.300027	-1446.2629
POP-3n	-1444.5963	0.393724	-1444.1764	0.07777	-1444.250439	-1446.2254
POP-3n_ra	-1444.6754	0.390725	-1444.2582	0.078492	-1444.333229	-1446.3628
POP-3n_ra-CO2	-1633.0626	0.40395	-1632.6282	0.088708	-1632.711557	-1634.97
POP-3n-CO2_ra	-1633.0496	0.405636	-1632.6152	0.083509	-1632.694635	-1634.9572
POP-3n-CO_radical	-1557.1235	0.390927	-1556.7064	0.077591	-1556.780179	-1558.8836

## References:

### Full reference Gaussian 16:

Gaussian 16, Revision B.01, Frisch, M. J.; Trucks, G. W.; Schlegel, H. B.; Scuseria, G. E.; Robb, M. A.; Cheeseman, J. R.; Scalmani, G.; Barone, V.; Mennucci, B.; Petersson, G. A.; Nakatsuji, H.; Caricato, M.; Li, X.; Hratchian, H. P.; Izmaylov, A. F.; Bloino, J.; Zheng, G.; Sonnenberg, J. L.; Hada, M.; Ehara, M.; Toyota, K.; Fukuda, R.; Hasegawa, J.; Ishida, M.; Nakajima, T.; Honda, Y.; Kitao, O.; Nakai, H.; Vreven, T.; Montgomery Jr., J. A.; Peralta, J. E.; Ogliaro, F.; Bearpark, M.; Heyd, J. J.; Brothers, E.; Kudin, K. N.; Staroverov, V. N.; Kobayashi, R.; Normand, J.; Raghavachari, K.; Rendell, A.; Burant, J. C.; Iyengar, S. S.; Tomasi, J.; Cossi, M.; Rega, N.; Millam, J. M.; Klene, M.; Knox, J. E.; Cross, J. B.; Bakken, V.; Adamo, C.; Jaramillo, J.; Gomperts, R.; Stratmann, R. E.; Yazyev, O.; Austin, A. J.; Cammi, R.; Pomelli, C.; Ochterski, J. W.; Martin, R. L.; Morokuma, K.; Zakrzewski, V. G.; Voth, G. A.; Salvador, P.; Dannenberg, J. J.; Dapprich, S.; Daniels, A. D.; Farkas, Ö.; Foresman, J. B.; Ortiz, J. V.; Cioslowski, J.; Fox, D. J. Gaussian, Inc., Wallingford CT, 2016.

- (1) Traxler, M.; Reischauer, S.; Vogl, S.; Roeser, J.; Rabeah, J.; Penschke, C.; Saalfrank, P.; Pieber, B.; Thomas, A. Programmable Photocatalytic Activity of Multicomponent Covalent Organic Frameworks Used as Metallaphotocatalysts. *Chem. – A Eur. J.* **2023**, *29* (4). <https://doi.org/10.1002/chem.202202967>.
- (2) Cui, D.; Wang, L.; Xu, K.; Ren, L.; Wang, L.; Yu, Y.; Du, Y.; Hao, W. Band-Gap Engineering of BiOCl with Oxygen Vacancies for Efficient Photooxidation Properties under Visible-Light Irradiation. *J. Mater. Chem. A* **2018**, *6* (5), 2193–2199. <https://doi.org/10.1039/C7TA09897A>.
- (3) Frisch, M. J. ; Trucks, G. W. ; Schlegel, H. B. ; Scuseria, G. E. ; Robb, M. A. ; Cheeseman, J. R. ; Scalmani, G. ; Barone, V. ; Petersson, G. A. ; Nakatsuji, H. ; Li, X. ; Caricato, M. ; Marenich, A. V. ; Bloino, J. ; Janesko, B. G. ; Gomperts, R. ; Mennucci, B. ; Hratch, D. J. Gaussian 16, Revision B.01. 2016.
- (4) Zhao, Y.; Truhlar, D. G. The M06 Suite of Density Functionals for Main Group Thermochemistry, Thermochemical Kinetics, Noncovalent Interactions, Excited States, and Transition Elements: Two New Functionals and Systematic Testing of Four M06-Class Functionals and 12 Other Function. *Theor. Chem. Acc.* **2008**, *120* (1), 215–241. <https://doi.org/10.1007/s00214-007-0310-x>.
- (5) Weigend, F.; Ahlrichs, R. Balanced Basis Sets of Split Valence, Triple Zeta Valence and Quadruple Zeta Valence Quality for H to Rn: Design and Assessment of Accuracy. *Phys. Chem. Chem. Phys.* **2005**, *7* (18), 3297–3305. <https://doi.org/10.1039/b508541a>.
- (6) Weigend, F. Accurate Coulomb-Fitting Basis Sets for H to Rn. *Phys. Chem. Chem. Phys.* **2006**, *8* (9), 1057–1065. <https://doi.org/10.1039/B515623H>.
- (7) Zhang, X.; Paton, R. S. Stereoretention in Styrene Heterodimerisation Promoted by One-Electron Oxidants. *Chem. Sci.* **2020**, *11* (34), 9309–9324. <https://doi.org/10.1039/d0sc03059g>.
- (8) Yang, X.; Xie, Y.; Xu, J.; Ren, S.; Mondal, B.; Zhou, L.; Tian, W.; Zhang, X.; Hao, L.; Jin, Z.; Chi, Y. R. Carbene-Catalyzed Activation of Remote Nitrogen Atoms of (Benz)Imidazole-Derived Aldimines for Enantioselective Synthesis of Heterocycles. *Angew. Chemie Int. Ed.* **2021**, *60* (14), 7906–7912. <https://doi.org/10.1002/anie.202016506>.
- (9) Song, R.; Liu, Y.; Majhi, P. K.; Ng, P. R.; Hao, L.; Xu, J.; Tian, W.; Zhang, L.; Liu, H.; Zhang, X.; Chi, Y. R. Enantioselective Modification of Sulfonamides and Sulfonamide-Containing Drugs: Via Carbene Organic Catalysis. *Org. Chem. Front.* **2021**, *8* (11), 2413–2419. <https://doi.org/10.1039/d1qo00212k>.
- (10) Lv, Y.; Luo, G.; Liu, Q.; Jin, Z.; Zhang, X.; Chi, Y. R. Catalytic Atroposelective Synthesis of Axially Chiral Benzonitriles via Chirality Control during Bond Dissociation and CN Group Formation. *Nat. Commun.* **2022**, *13* (1), 1–9. <https://doi.org/10.1038/s41467-021-27813-4>.
- (11) Deng, R.; Wu, S.; Mou, C.; Liu, J.; Zheng, P.; Zhang, X.; Chi, Y. R. Carbene-Catalyzed Enantioselective Sulfonylation of Enone Aryl Aldehydes: A New Mode of Breslow Intermediate Oxidation. *J. Am. Chem. Soc.* **2022**, *144* (12), 5441–5449. <https://doi.org/10.1021/jacs.1c13384>.
- (12) Lv, W. X.; Chen, H.; Zhang, X.; Ho, C. C.; Liu, Y.; Wu, S.; Wang, H.; Jin, Z.; Chi, Y. R.

- Programmable Selective Acylation of Saccharides Mediated by Carbene and Boronic Acid. *Chem***2022**, 8 (5), 1518–1534. <https://doi.org/10.1016/j.chempr.2022.04.019>.
- (13) Yang, X.; Wei, L.; Wu, Y.; Zhou, L.; Zhang, X.; Chi, Y. R. Atroposelective Access to 1,3-Oxazepine-Containing Bridged Biaryls via Carbene-Catalyzed Desymmetrization of Imines. *Angew. Chemie Int. Ed.***2022**, 62 (1), e202211977. <https://doi.org/10.1002/anie.202211977>.
- (14) Wei, L.; Li, J.; Zhao, Y.; Zhou, Q.; Wei, Z.; Chen, Y.; Zhang, X.; Yang, X. Chiral Phosphoric Acid Catalyzed Asymmetric Hydrolysis of Biaryl Oxazepines for the Synthesis of Axially Chiral Biaryl Amino Phenol Derivatives. *Angew. Chemie Int. Ed.***2023**, 62 (39), e202306864. <https://doi.org/10.1002/ANIE.202306864>.
- (15) Luo, Z.; Liao, M.; Li, W.; Zhao, S.; Tang, K.; Zheng, P.; Chi, Y. R.; Zhang, X.; Wu, X. Ionic Hydrogen Bond-Assisted Catalytic Construction of Nitrogen Stereogenic Center via Formal Desymmetrization of Remote Diols. *Angew. Chemie Int. Ed.***2024**, e202404979. <https://doi.org/10.1002/ANIE.202404979>.
- (16) Barone, V.; Cossi, M. Quantum Calculation of Molecular Energies and Energy Gradients in Solution by a Conductor Solvent Model. *J. Phys. Chem. A***1998**, 102 (11), 1995–2001. <https://doi.org/10.1021/jp9716997>.
- (17) Cossi, M.; Rega, N.; Scalmani, G.; Barone, V. Energies, Structures, and Electronic Properties of Molecules in Solution with the C-PCM Solvation Model. *J. Comput. Chem.***2003**, 24 (6), 669–681. <https://doi.org/10.1002/jcc.10189>.
- (18) Gagliardi, L. G.; Castells, C. B.; Ràfols, C.; Rosés, M.; Bosch, E. Static Dielectric Constants of Acetonitrile/Water Mixtures at Different Temperatures and Debye-Hückel A and A0B Parameters for Activity Coefficients. *J. Chem. Eng. Data***2007**, 52 (3), 1103–1107. [https://doi.org/10.1021/JE700055P/SUPPL\\_FILE/JE700055P-FILE002.PDF](https://doi.org/10.1021/JE700055P/SUPPL_FILE/JE700055P-FILE002.PDF).
- (19) Grimme, S. Supramolecular Binding Thermodynamics by Dispersion-Corrected Density Functional Theory. *Chem. - A Eur. J.***2012**, 18 (32), 9955–9964. <https://doi.org/10.1002/chem.201200497>.
- (20) Luchini, G.; Alegre-Requena, J. V.; Funes-Ardoiz, I.; Paton, R. S. GoodVibes: Automated Thermochemistry for Heterogeneous Computational Chemistry Data. *FI000Research***2020**, 9, 291. <https://doi.org/10.12688/fi000research.22758.1>.
- (21) Bryantsev, V. S.; Diallo, M. S.; Goddard Iii, W. A.; Goddard, W. A. Calculation of Solvation Free Energies of Charged Solutes Using Mixed Cluster/Continuum Models. *J. Phys. Chem. B***2008**, 112 (32), 9709–9719.
- (22) Yanai, T.; Tew, D. P.; Handy, N. C. A New Hybrid Exchange–Correlation Functional Using the Coulomb-Attenuating Method (CAM-B3LYP). *Chem. Phys. Lett.***2004**, 393 (1–3), 51–57. <https://doi.org/10.1016/J.CPLETT.2004.06.011>.
- (23) Peach, M. J. G.; Benfield, P.; Helgaker, T.; Tozer, D. J. Excitation Energies in Density Functional Theory: An Evaluation and a Diagnostic Test. *J. Chem. Phys.***2008**, 128 (4), 044118. <https://doi.org/10.1063/1.2831900>.
- (24) Jacquemin, D.; Wathelet, V.; Perpète, E. A.; Adamo, C. Extensive TD-DFT Benchmark: Singlet-Excited States of Organic Molecules. *J. Chem. Theory Comput.***2009**, 5 (9), 2420–2435. <https://doi.org/10.1021/ct900298e>.
- (25) Stauber, J. M.; Schwan, J.; Zhang, X.; Axtell, J. C.; Jung, D.; McNicholas, B. J.; Oyala, P. H.; Martinolich, A. J.; Winkler, J. R.; See, K. A.; Miller, T. F.; Gray, H. B.; Spokoyny, A. M. A Super-Oxidized Radical Cationic Icosahedral Boron Cluster. *J. Am. Chem. Soc.***2020**, 142 (30), 12948–12953. [https://doi.org/10.1021/JACS.0C06159/SUPPL\\_FILE/JA0C06159\\_SI\\_001.PDF](https://doi.org/10.1021/JACS.0C06159/SUPPL_FILE/JA0C06159_SI_001.PDF).
- (26) Li, B.; Zhang, X.; Stauber, J. M.; Miller, T. F.; Spokoyny, A. M. Electronic Structure of Superoxidized Radical Cationic Dodecaborate-Based Clusters. *J. Phys. Chem. A***2021**, 125 (28), 6141–6150. [https://doi.org/10.1021/ACS.JPCA.1C03927/SUPPL\\_FILE/JP1C03927\\_SI\\_001.PDF](https://doi.org/10.1021/ACS.JPCA.1C03927/SUPPL_FILE/JP1C03927_SI_001.PDF).
- (27) Hellweg, A.; Rappoport, D. Development of New Auxiliary Basis Functions of the Karlsruhe Segmented Contracted Basis Sets Including Diffuse Basis Functions (Def2-SVPD, Def2-TZVPPD, and Def2-QVPPD) for RI-MP2 and RI-CC Calculations. *Phys. Chem. Chem. Phys.***2014**, 17 (2), 1010–1017. <https://doi.org/10.1039/C4CP04286G>.
- (28) Davidson, E. R.; Feller, D. Basis Set Selection for Molecular Calculations. *Chem. Rev.***1986**,

- 86 (4), 681–696. <https://doi.org/10.1021/CR00074A002>.
- (29) Lynch, B. J.; Zhao, Y.; Truhlar, D. G. Effectiveness of Diffuse Basis Functions for Calculating Relative Energies by Density Functional Theory. *J. Phys. Chem. A* **2003**, *107* (9), 1384–1388. <https://doi.org/10.1021/JP021590L>.
- (30) Papajak, E.; Zheng, J.; Xu, X.; Leverentz, H. R.; Truhlar, D. G. Perspectives on Basis Sets Beautiful: Seasonal Plantings of Diffuse Basis Functions. *J. Chem. Theory Comput.* **2011**, *7* (10), 3027–3034. <https://doi.org/10.1021/CT200106A>.
- (31) Gaussian. *Creating UV/Visible Plots from the Results of Excited States Calculations* | *Gaussian.com*.
- (32) Schrödinger, L. *The PyMOL Molecular Graphics Development Component, Version 1.8*; 2015.
- (33) Zou, W.; Cheng, Y.; Ye, Y.; Wei, X.; Tong, Q.; Dong, L.; Ouyang, G. Metal-Free Photocatalytic CO<sub>2</sub> Reduction to CH<sub>4</sub> and H<sub>2</sub>O<sub>2</sub> under Non-sacrificial Ambient Conditions. *Angew. Chemie Int. Ed.* **2023**, *62* (49). <https://doi.org/10.1002/anie.202313392>.
- (34) Hou, Y.; Zhang, E.; Gao, J.; Zhang, S.; Liu, P.; Wang, J.-C.; Zhang, Y.; Cui, C.-X.; Jiang, J. Metal-Free Azo-Bridged Porphyrin Porous Organic Polymers for Visible-Light-Driven CO<sub>2</sub> Reduction to CO with High Selectivity. *Dalt. Trans.* **2020**, *49* (22), 7592–7597. <https://doi.org/10.1039/D0DT01436B>.
- (35) Lei, K.; Wang, D.; Ye, L.; Kou, M.; Deng, Y.; Ma, Z.; Wang, L.; Kong, Y. A Metal-Free Donor–Acceptor Covalent Organic Framework Photocatalyst for Visible-Light-Driven Reduction of CO<sub>2</sub> with H<sub>2</sub>O. *ChemSusChem* **2020**, *13* (7), 1725–1729. <https://doi.org/10.1002/cssc.201903545>.
- (36) Cui, J.-X.; Wang, L.-J.; Feng, L.; Meng, B.; Zhou, Z.-Y.; Su, Z.-M.; Wang, K.; Liu, S. A Metal-Free Covalent Organic Framework as a Photocatalyst for CO<sub>2</sub> Reduction at Low CO<sub>2</sub> Concentration in a Gas–Solid System. *J. Mater. Chem. A* **2021**, *9* (44), 24895–24902. <https://doi.org/10.1039/D1TA07686H>.
- (37) Mondal, S.; Powar, N. S.; Paul, R.; Kwon, H.; Das, N.; Wong, B. M.; In, S.-I.; Mondal, J. Nanoarchitectonics of Metal-Free Porous Polyketone as Photocatalytic Assemblies for Artificial Photosynthesis. *ACS Appl. Mater. Interfaces* **2022**, *14* (1), 771–783. <https://doi.org/10.1021/acsami.1c18626>.
- (38) Dai, C.; Zhong, L.; Gong, X.; Zeng, L.; Xue, C.; Li, S.; Liu, B. Triphenylamine Based Conjugated Microporous Polymers for Selective Photoreduction of CO<sub>2</sub> to CO under Visible Light. *Green Chem.* **2019**, *21* (24), 6606–6610. <https://doi.org/10.1039/C9GC03131F>.
- (39) Wen, F.; Zhang, F.; Wang, Z.; Yu, X.; Ji, G.; Li, D.; Tong, S.; Wang, Y.; Han, B.; Liu, Z. Amide-Bridged Conjugated Organic Polymers: Efficient Metal-Free Catalysts for Visible-Light-Driven CO<sub>2</sub> Reduction with H<sub>2</sub>O to CO. *Chem. Sci.* **2021**, *12* (34), 11548–11553. <https://doi.org/10.1039/D1SC02499J>.
- (40) Jena, R.; Rahimi, F. A.; Mandal, T.; Das, T. N.; Parambil, S. R. V.; Mondal, S. K.; Maji, T. K. Photocatalytic CO<sub>2</sub> Reduction to Solar Fuels by a Chemically Stable Bimetallic Porphyrin-Based Framework. *Inorg. Chem.* **2024**, *63* (38), 17836–17845. <https://doi.org/10.1021/acs.inorgchem.4c02841>.
- (41) Wang, L.; Wang, R.; Zhang, X.; Mu, J.; Zhou, Z.; Su, Z. Improved Photoreduction of CO<sub>2</sub> with Water by Tuning the Valence Band of Covalent Organic Frameworks. *ChemSusChem* **2020**, *13* (11), 2973–2980. <https://doi.org/10.1002/cssc.202000103>.
- (42) Ye, W.; Wang, Y.; Ji, G.; Zhang, F.; Zhao, Y.; Liu, Z. Carbazolic Conjugated Organic Polymers for Visible-Light-Driven CO<sub>2</sub> Photoreduction with H<sub>2</sub>O to CO with High Efficiency and Selectivity. *ChemSusChem* **2022**, *15* (16). <https://doi.org/10.1002/cssc.202200759>.
- (43) Yang, L.; Yan, W.; Yang, N.; Wang, G.; Bi, Y.; Tian, C.; Liu, H.; Zhu, X. Regulating  $\pi$ -Conjugation in Sp<sup>2</sup>-Carbon-Linked Covalent Organic Frameworks for Efficient Metal-Free CO<sub>2</sub> Photoreduction with H<sub>2</sub>O. *Small* **2023**, *19* (27). <https://doi.org/10.1002/smll.202208118>.